A numerical study of a particular non-conservative hyperbolic problem [⋆]

V. Dolejší [a,b,*], T. Gallouët [b]

[a]*Charles University Prague, Faculty of Mathematics and Physics, Sokolovská 83, 186 75 Prague, Czech Republic*

[b] *Laboratoire d'Analyse Topologie et Probabilités, UMR CNRS 6632, Centre de Mathématiques et Informatique, Université de Provence, 39 rue Joliot Curie, 13453 Marseille, France*

Abstract

We study the ability of several numerical schemes to solve a non-conservative hyperbolic system arising from a flow simulation of solid-liquid-gas slurries with the so-called virtual mass effect. Two classes of numerical schemes are used: some Roe-type finite volume schemes, which are based on the resolution of linearized Riemann problems, and some (centered or upwind) schemes with an additional artificial diffusion, such as the classical Rusanov scheme. For flow regimes of interest (steady as well as unsteady flows), the computational process breaks down for some schemes. Indeed, for such flows, the system has at least one eigenvalue having a small magnitude in the interior of the computational domain and this a possible reason for the failure of some upwind schemes using the resolution of a linearized Riemann problem. Such a failure does not appear with, for instance, the Rusanov scheme which is well known for its robustness. Furthermore, since the system is nonconservative, it is not clear what a weak solution is, when the solution is discontinuous (at least, one needs to have the nonconservative equivalent of the Rankine-Hugoniot jump conditions) and we show that the approximate solution given by different numerical schemes converges towards different "weak solutions".

Key words: three phase flow; virtual mass effect; non-conservative hyperbolic system; FV Roe scheme with non-conservative variables
PACS:

1 Introduction

Our aim is to simulate the flow of a solid-liquid-gas slurry, which can be used, e.g., for the transport of a mixture of sand, oil and air in a pipe. The complete model is based on the so-called virtual mass effect. It can be found, for instance, in [1], [2]. This model belongs to the class of non-conservative hyperbolic problems with source terms, which can be written (for one space dimension) in the form

$$\frac{\partial \boldsymbol{w}}{\partial t} + \boldsymbol{C}(\boldsymbol{w})\frac{\partial \boldsymbol{w}}{\partial x} = \boldsymbol{S}(\boldsymbol{w}), \quad x \in (0, L), \, t \in (0, T), \tag{1}$$

where $\boldsymbol{w} = \boldsymbol{w}(x, t) : (0, L) \times (0, T) \to I\!\!R^N$, $\boldsymbol{C}(\boldsymbol{w}) : (0, L) \times (0, T) \to I\!\!R^{N^2}$ is a $N \times N$ matrix and $\boldsymbol{S}(w) : (0, L) \times (0, T) \to I\!\!R^N$ is a vector representing source terms. Firstly we solved this problem with the aid of the centred Rusanov scheme [3] in the papers [4] and [5]. Although systems of type (1) describe many physical processes (e.g., multiphase flow, shallow-water problems) our model is rather particular. For flow regimes of interest, various numerical schemes, using upwinding and the resolution of linearized Riemann problems, give unphysical numerical solutions and the computational processes fail. It seems to be due by the fact that at least one eigenvalue of the matrix $\boldsymbol{C}(\boldsymbol{w})$ has a small magnitude (in particular, it makes matrix $\boldsymbol{C}(\boldsymbol{W})$ very sensitive with respect to the components of $\boldsymbol{W}$ and to the rounding errors). Consequently, the *first purpose* of this paper is to describe this phenomenon, demonstrate it by numerical experiments and present numerical schemes which do not suffer from the mentioned effect.

The concept of a weak solution of the non-conservative system (1) is not well defined if the solution contains discontinuities. In order to define what is a solution of a non-conservative system, it is, at least, necessary to prescribe additionally some jump conditions. In the case of a conservative system, these jump conditions are implicitly given and consequently, any stable conservative scheme converges to a weak solution, which satisfies the "strong" form of the conservative system in the regular zones and the jump conditions for discontinuities.

* Corresponding author, Charles University Prague, Faculty of Mathematics and Physics, Sokolovská 83, 186 75 Prague, Czech Republic, tel: +420221913373, fax: +420224810136

Email addresses: dolejsi@karlin.mff.cuni.cz (V. Dolejší), gallouet@cmi.univ-mrs.fr (T. Gallouët).

In our non-conservative problem, the jump conditions are not prescribed. These jump conditions could be given, for instance, with the form of a neglected viscosity term (as in [6] and [7]). But this viscosity term seems to be not available. Since the model is interesting from a practical point of view, we deal with its numerical solution although the relevant mathematical theory does not allow us to determine what a weak solution is. The numerical experiments should be used to try to give a sense what a weak solution should be. The *second interest* of this paper is to remark that for the non-conservative system the limit of approximate solutions given by a stable scheme may depend on this scheme. More precisely, the limit of approximate solutions (given by different schemes) differ from the speed of propagation of discontinuities.

There exist a lot of papers dealing with a solution of (1) with the aid of various numerical schemes. Very popular are upwind schemes based on the solution of the local Riemann problem at each interface of the mesh. Since the computation of the exact solution of the local Riemann problem is difficult and expensive for complicated systems (and not well defined, in our case...), schemes based on approximate Riemann solvers were introduced. For a survey see, e.g., [8], [9], [10], [11], [12]. The linearized approximate Riemann solver of Roe [13] was proposed in 1981 for the numerical solution of hyperbolic conservation laws. A weak formulation of Roe's approximate Riemann solver, based on the choice of a path in the states space, has been introduced in [14]. This weak formulation was applied in order to build a Roe-averaged matrix for a conservative system governing a homogeneous equilibrium two-phase flow. A generalization of this formulation to a hyperbolic non-conservative system modelling a two-component two-phase flow was carried out in [15]. However, the complexity of the considered model (defined in Section 2) gives no chance to apply this approach since we are not able to evaluate an integration along a suitable path in the states space. Another approach was used in [16] for the solution of a two-fluids model, for comparison see [17]. Also for this method, the complexity of the considered model does not enable to perform some matrix operations analytically and their numerical realization leads to unsatisfactory results.

Therefore, we deal with an alternative to the Roe scheme, the "Finite volume Roe scheme" which was introduced in [18] to approximate solution of a two-phase flow. Indeed, we use a variant of this scheme, called VFRoe-ncv ("volumes finis" Roe with non-conservative variables) scheme, which was applied for the solution of the Euler equations in [19], for the solution of shallow-water equations with topography in [20] and for two-phase flow in [21]. VFRoe-ncv scheme is based on the solution of the linearized Riemann problem at each mesh interface in non-conservative variables. A similar approach was applied in [22] for modelling of two-phase flows where a modification of the Roe scheme was used.

An application of VFRoe-ncv schemes causes some troubles. We observe that if some eigenvalue of $\boldsymbol{C}$ in (1) has a small magnitude then the solution of the linearized Riemann problem can be unphysical which causes the failure of the computation process. However, we present numerical schemes which are able to solve the considered problem. Nevertheless, different numerical schemes converge to different weak solutions. It is caused by the non-conservativity of the system where additional (jump) condition on discontinuities have to be added in order to prescribe the speed of propagation of the discontinuities. (Furthermore, some entropy conditions are also useful to determine the admissibility of a discontinuity.)

The content of the rest of this paper is the following. In Section 2, we present the model with some of its properties and we also discuss boundary conditions for steady and unsteady flows. In Section 3, we present several schemes for the solution of solid-liquid-gas slurry flows. The capability of the schemes to compute steady as well as unsteady flow problems and the non-uniqueness of the limit of approximate solutions are discussed in Section 4. Finally, we give some concluding remarks at the end of the paper.

2   Considered problem

2.1   Governing equations

A description and a derivation of the model of the flow of a solid-liquid-gas slurries in a pipe can be found in [1] and [2]. Based on the observation that the liquid and gas phases of the mixture adhere to solid particles, the so-called *virtual mass effect* is included in the model. For simplicity, we slightly modified the equation by neglecting partial derivatives of pressure with respect to space, for argumentation and details see [4].

In this paper, we deal with the following problem. Let $(0, L)$ be a computational domain representing a pipe and $T > 0$ be a final time of interest. We seek a vector function $\boldsymbol{w}(x, t) : (0, L) \times (0, T) \rightarrow \mathrm{PAS} \subset I\!\!R^5$ such that

$$\tilde{\boldsymbol{A}}(\boldsymbol{w})\frac{\partial \boldsymbol{w}}{\partial t} + \frac{\partial \tilde{\boldsymbol{f}}(\boldsymbol{w})}{\partial x} + \tilde{\boldsymbol{C}}(\boldsymbol{w})\frac{\partial \boldsymbol{w}}{\partial x} = \tilde{\boldsymbol{S}}(\boldsymbol{w}), \quad x \in (0, L),\ t \in (0, T), \qquad (2)$$

where

$$\boldsymbol{w} = (U_\ell, U_s, C_\ell, C_s, P)^{\mathrm{T}}, \tag{3}$$

$$
\tilde{\boldsymbol{A}}(\boldsymbol{w}) = \begin{pmatrix} \overline{C}_\ell \overline{\rho}_\ell & 0 & 0 & 0 & 0 \\ 0 & \overline{C}_s \overline{\rho}_s & 0 & 0 & 0 \\ 0 & 0 & 1 & 0 & \frac{C_\ell}{\rho_\ell a_\ell^2} \\ 0 & 0 & -1 & -1 & \frac{C_g}{\rho_g a_g^2} \\ 0 & 0 & 0 & 1 & \frac{C_s}{\rho_s a_s^2} \end{pmatrix}, \quad
\tilde{\boldsymbol{S}}(\boldsymbol{w}) = \begin{pmatrix} -\overline{\rho}_\ell \left(g\overline{C}_\ell \frac{\mathrm{d}z}{\mathrm{d}x} + I_\ell + I_{\ell s} \right) \\ -\overline{\rho}_s \left(g\overline{C}_s \frac{\mathrm{d}z}{\mathrm{d}x} - I_{\ell s} \right) \\ 0 \\ 0 \\ 0 \end{pmatrix},
$$

$$
\tilde{\boldsymbol{f}}(\boldsymbol{w}) = \begin{pmatrix} \overline{C}_\ell P \\ \overline{C}_s P \\ (1 - K_{\ell s})C_\ell U_\ell + K_{\ell s}C_\ell U_s \\ (1 - K_{gs})C_g U_\ell + K_{gs}C_g U_s \\ C_s U_s \end{pmatrix}, \quad
\tilde{\boldsymbol{C}}(\boldsymbol{w}) = \begin{pmatrix} \overline{C}_\ell \overline{\rho}_\ell U_\ell & 0 & 0 & 0 & 0 \\ 0 & \overline{C}_s \overline{\rho}_s U_s & 0 & 0 & 0 \\ 0 & 0 & 0 & 0 & 0 \\ 0 & 0 & 0 & 0 & 0 \\ 0 & 0 & 0 & 0 & 0 \end{pmatrix},
$$

the indexes $_s$, $_\ell$ and $_g$ denote the solid, liquid and gas phases, P is the pressure of the slurry, ρ_k, C_k, K_k and a_k are the density, volume fraction, velocity and wave speed of the k-phase, respectively. The volume fractions satisfy the relation $C_s + C_\ell + C_g = 1$.

Further, introducing the virtual mass effect, the part of the slurry which moves with the velocity of solid phase U_s is given by $\overline{C}_s = C_s + K_{\ell s}C_\ell + K_{gs}C_g$, and the rest of the slurry $\overline{C}_\ell = (1 - K_{\ell s})C_\ell + (1 - K_{gs})C_g$ moves with the velocity of the liquid phase U_ℓ, where $K_{\ell s}$ and K_{gs} represent a relative adhesion of the liquid and gas parts of the slurry to the solid particles, respectively. The coefficients $K_{\ell s}$ and K_{gs} are not constant but depend on the volume fractions. In [1], [2], the following $K_{\ell s}C_\ell = (K_1 + K_2 C_s)C_s$ and $K_{gs}C_g = K_3 C_g$, with $K_1 = K_3 = 0.5$, $K_2 = 0.25$. Furthermore, the averaged densities are given by

$$
\overline{\rho}_s = \frac{1}{\overline{C}_s} \left(C_s \rho_s + K_{\ell s}C_\ell \rho_\ell + K_{gs}C_g \rho_g \right), \tag{4}
$$
$$
\overline{\rho}_\ell = \frac{1}{\overline{C}_\ell} \left((1 - K_{\ell s})C_\ell \rho_\ell + (1 - K_{gs})C_g \rho_g \right).
$$

Moreover, the function $z = z(x)$ in (3) gives the position of the pipe above a horizontal ground, g is the gravity and the terms I_ℓ and $I_{\ell s}$ represent the hydraulic losses given by

$$
I_\ell = \frac{f_\ell}{2D} U_\ell |U_\ell|, \quad I_{\ell s} = \frac{3}{4} \frac{C_s C_D}{d} (U_\ell - U_s)|U_\ell - U_s| \tag{5}
$$

where the quantity f_ℓ is the friction coefficient (supposed to be constant), D is the inner pipe diameter, C_D is the drag coefficient, d is the size of solid

particles.

Finally, PAS denotes a set of *Physically Admissible Solutions* satisfying

$$\text{PAS} = \{\boldsymbol{w} = (w_1, \ldots, w_5), \ w_3 \geq 0, \ w_4 \geq 0, \ w_3 + w_4 \leq 1, \ w_5 \geq 0\}. \quad (6)$$

The system of equations (2) – (3) can be rewritten in the form corresponding with (1) by

$$\frac{\partial \boldsymbol{w}}{\partial t} + \boldsymbol{C}(\boldsymbol{w})\frac{\partial \boldsymbol{w}}{\partial x} = \boldsymbol{S}(\boldsymbol{w}), \quad x \in (0, L), \ t \in (0, T), \quad (7)$$

where $\boldsymbol{C}(\boldsymbol{w}) \equiv \tilde{\boldsymbol{A}}^{-1}(\boldsymbol{w})\left[\tilde{\boldsymbol{J}}(\boldsymbol{w}) + \tilde{\boldsymbol{C}}(\boldsymbol{w})\right]$, $\boldsymbol{S}(\boldsymbol{w}) \equiv \tilde{\boldsymbol{A}}^{-1}(\boldsymbol{w})\tilde{\boldsymbol{S}}(\boldsymbol{w})$ and $\tilde{\boldsymbol{J}}(\boldsymbol{w})$ denotes the Jacobian matrix of $\tilde{\boldsymbol{f}}(\boldsymbol{w})$. Matrixes $\tilde{\boldsymbol{A}}^{-1}(\cdot)$ and $\tilde{\boldsymbol{J}}(\cdot)$ can be simply evaluated analytically.

The system of equations (7) is supplemented by an initial condition $\boldsymbol{w}(x, 0) = \boldsymbol{w}^0(x), \ x \in (0, L), \ (\boldsymbol{w}^0 : (0, L) \to \text{PAS}$ is a given function) and by suitable boundary conditions formally written $B(\boldsymbol{w}(x, t)) = 0, \ x = 0, \ x = L$, which are discussed in Section 2.4.

In this paper we deal with the numerical simulation of two flow regimes:

- The simulation of a *steady state* flow of slurry in a pipe. This flow regime corresponds to a real situation where at the inlet of the pipe, there is a reservoir of slurry with phase fractions C_ℓ^I, C_s^I and $C_g^I(= 1 - C_s^I - C_\ell^I)$ and pressure P^I. At the outlet of the pipe, there is the second reservoir of slurry with pressure P^O $(P^O < P^I)$. If the outlet reservoir is empty (free outlet), we set $P^O = 0$. Based on physical considerations this flow configuration leads to a steady state solution with constant fractions and velocities and linearly decreasing pressure.
- The simulation of the so called *water hammer*. Here the steady state solution from the previous case is supposed to be the initial condition and at time $t = 0$ the outlet of the pipe is closed. This effect leads to an unsteady flow when the velocities U_ℓ and U_s are vanishing from the closed end of the pipe. Moreover, the pressure as well as the fractions of heavier solid and liquid particles are increasing whereas the fraction of gas goes fast to a very small value tending to zero. These changes of fractions, velocities and pressure propagate inside the pipe in opposite direction as the velocity of the main steady state flow.

6

Remark 1   As we mentioned at the beginning of this paper the non-conservativity of the system (7) causes a lot of troubles, namely an impossibility to easily define a weak solution. Then a natural question arises: it is possible to formulate the considered model in a conservation form? The first obstacle represents the use of the virtual mass effect which was derived in a non-conservative form, see [1], [2].

However, even in case of a simple model the reformulation of a non-conservative problem to a conservative one is possible only if some additional information is available. For simplicity, let us consider the Burgers equation in the non-conservative form

$$\frac{\partial u}{\partial t} + u\frac{\partial u}{\partial x} = 0, \qquad x \in \mathbb{R},\ t \geq 0. \tag{8}$$

The equation (8) is equivalent (for regular solutions) with the equation

$$\frac{\partial u}{\partial t} + \frac{\partial}{\partial x}\left(\frac{u^2}{2}\right) = 0, \tag{9}$$

and assuming that $u \geq 0$ also with, e.g.,

$$\frac{\partial v}{\partial t} + \frac{\partial}{\partial x}\left(\frac{2v^{3/2}}{3}\right) = 0, \quad \text{where } v \equiv u^2. \tag{10}$$

Although equations (9) and (10) are equivalent for a continuous solution, they are different if the solution is discontinuous since both equations correspond to different Rankine-Hugoniot conditions. Thus the non-conservative equation (8) can be written uniquely in a conservative form only if some additional information (defining uniquely the Rankine-Hugoniot conditions) is given. But such a type of information (following from a physical aspect) seems not to be available for the model of the three phase flow with the virtual mass effect.

Remark 2   Let us note that if $\boldsymbol{w}$ is a discontinuous function then the non-conservative term

$$\boldsymbol{C}(\boldsymbol{w})\frac{\partial \boldsymbol{w}}{\partial x} \tag{11}$$

lacks meaning as the distribution and the usual theory of hyperbolic systems of conservation laws does not apply. There are several possibilities how to give a unique meaning to (11). In [23], an integration along a suitable path is used

for the definition of (11). The approach presented in [24] relies on the form of matrix $\boldsymbol{C}$: some equations of the system

$$\frac{\partial \boldsymbol{w}}{\partial t} + \boldsymbol{C}(\boldsymbol{w})\frac{\partial \boldsymbol{w}}{\partial x} = 0, \tag{12}$$

are considered in a strong sense and the other in a weak sense. In [6] and [7], the author adds to (12) a diffusive term $-\varepsilon\frac{\partial}{\partial x}(\boldsymbol{D}(\boldsymbol{w})\frac{\partial \boldsymbol{w}}{\partial x})$ ($\boldsymbol{D}(\boldsymbol{w})\boldsymbol{w}$ is a regular matrix) and the solution of (12) is defined as the limit of "diffusive solutions" when the diffusive term tends to zero ($\varepsilon \to 0$). However, the limit solution depends on the form of $\boldsymbol{D}(\boldsymbol{w})$.

In each case some extra information is added, an integration path in [23], a type of consideration of equations in [24] or a form of a diffusive term $\boldsymbol{D}$ in [6], [7]. Since problem (12) is non-conservative, the numerical treatments of the mentioned approaches lead to different numerical solutions.

Unfortunately, each of the presented approaches is too complicated to apply to the model (3) – (5). Thus, as mentioned in Section 1, we do not deal with the meaning of the non-conservative term (11) and the weak form of the system (7) any more. However, we observe that different schemes converge towards different "weak solutions" (solutions with different jump conditions).

2.3 Basic properties of system (7)

System (7) exhibits a strongly nonlinear non-conservative hyperbolic problem. The definition of the model (3) – (5) gives us no chance to analytically compute eigenvalues and eigenvectors of matrix $\boldsymbol{C}(\boldsymbol{w})$, $\boldsymbol{w} \in$ PAS. Based on numerical experiments we observe that the matrix $\boldsymbol{C}(\boldsymbol{w})$, $\boldsymbol{w} \in$ PAS has five real eigenvalues λ_l, $l = 1,\ldots,5$ (if $\boldsymbol{w} \notin$ PAS then $\boldsymbol{C}(\boldsymbol{w})$ has complex eigenvalues in general)

$$\lambda_1 = u, \quad \lambda_{2,3} = u \pm c_1, \quad \lambda_{4,5} = u \pm c_2, \tag{13}$$

where $u \in (\min(U_\ell, U_s), \ \max(U_\ell, U_s))$ depends on velocities, fractions and other model parameters but it is independent of pressure. Therefore $U_l = U_s$ implies $u = U_l = U_s$. The values c_1, c_2, $0 \leq c_1 < c_2$ are monotonically increasing functions of pressure and depend also on velocities, fractions and model parameters. Moreover, if the pressure is equal to zero then also $c_1 = 0$ so that $\lambda_1 = \lambda_2 = \lambda_3$ and system (7) is not strictly hyperbolic.

We observe that the matrix $\boldsymbol{C}(\boldsymbol{w})$ in (7) has at least one eigenvalue with a vanishing magnitude in the interior of the computational domain for both flow

8

regimes of interest.

- In case of a steady state flow simulation with an (almost) empty outlet reservoir (P^O is small), the velocities U_ℓ and U_s are positive and pressure (almost) vanishes at the outlet of the pipe. Then there exists a point $x \in (0, L)$ where $c_1 \approx u$ and consequently $\lambda_3 \approx 0$.
- In case of a simulation of the water hammer the outlet end of the pipe is closed, velocities U_ℓ and U_s are vanishing from the pipe outlet and consequently λ_1 also vanishes from the outlet of the pipe.

These properties are documented in Figure 1 where the eigenvalues of the matrices $\boldsymbol{C}(\boldsymbol{w}^{\text{steady}}(x))$, $x \in (0, L)$ and $\boldsymbol{C}(\boldsymbol{w}^{\text{wh}}(x, t))$, $x \in (0, L)$ for $t = 0.002\ s$, $t = 0.001\ s$ and $t = 0.05\ s$ are presented. The state vector $\boldsymbol{w}^{\text{steady}}(x)$, $x \in (0, L)$ denotes the steady state solution and $\boldsymbol{w}^{\text{wh}}(x, t))$, $x \in (0, L)$, $t \geq 0$ the unsteady solution of the water hammer, obviously $\boldsymbol{w}^{\text{wh}}(x, 0) \equiv \boldsymbol{w}^{\text{steady}}(x)$, $x \in (0, L)$.

2.4 Boundary conditions

We present the boundary conditions used for a computation of the steady state and water hammer flow regimes. We assume that slurry flows from left to right and thus the inlet and the outlet of the pipe are located at $x = 0$ and $x = L$, respectively. Some components of vector $\boldsymbol{w}$ have to be given by boundary conditions and the others have to be extrapolated from the interior of the computational domain. The number of prescribed components is equal to a number of negative values $\bar{\lambda}_l \equiv \lambda_l n$, $l = 1, \ldots, 5$, where λ_l, $l = 1, \ldots, 5$ are eigenvalues of $\boldsymbol{C}(\boldsymbol{w})$, n is a 1D variant of unit outer normal, i.e., $n = -1$ and $n = 1$ for left and right end points of $(0, L)$, respectively.

Let $U_\ell^{\text{I}-\text{ex}}$ and $U_s^{\text{I}-\text{ex}}$ denote the liquid and solid velocities extrapolated from the interior of the interval $(0, L)$ at the inlet $(x = 0)$, respectively. Similarly, let $U_\ell^{\text{O}-\text{ex}}$, $U_s^{\text{O}-\text{ex}}$, $C_\ell^{\text{O}-\text{ex}}$, $C_s^{\text{O}-\text{ex}}$ and $P^{\text{O}-\text{ex}}$ denote the velocities, volume fractions and pressure extrapolated from the interior of the interval $(0, L)$ at the outlet$(x = L)$, respectively. We use the following boundary conditions.

- *Pipe with open ends* (steady state solution): numerical examples show (see Figure 1, left) that the number of negative values $\bar{\lambda}_l$, $l = 1, \ldots, 5$ is equal to 3 at the inlet and 1 at the outlet. Based on the physical argumentation, we prescribe the values of pressure and volume fractions at the inlet and pressure at the outlet. The other components are extrapolated from the interior of the domain. It means that we put

$$\boldsymbol{w}(x = 0, t) = (U_\ell^{\text{I}-\text{ex}}, U_s^{\text{I}-\text{ex}}, C_\ell^I, C_s^I, P^I), \qquad t \in (0, T), \quad (14)$$

$$\boldsymbol{w}(x = L, t) = (U_\ell^{\text{O}-\text{ex}}, U_s^{\text{O}-\text{ex}}, C_\ell^{\text{O}-\text{ex}}, C_s^{\text{O}-\text{ex}}, P^O), \qquad t \in (0, T), \quad (15)$$
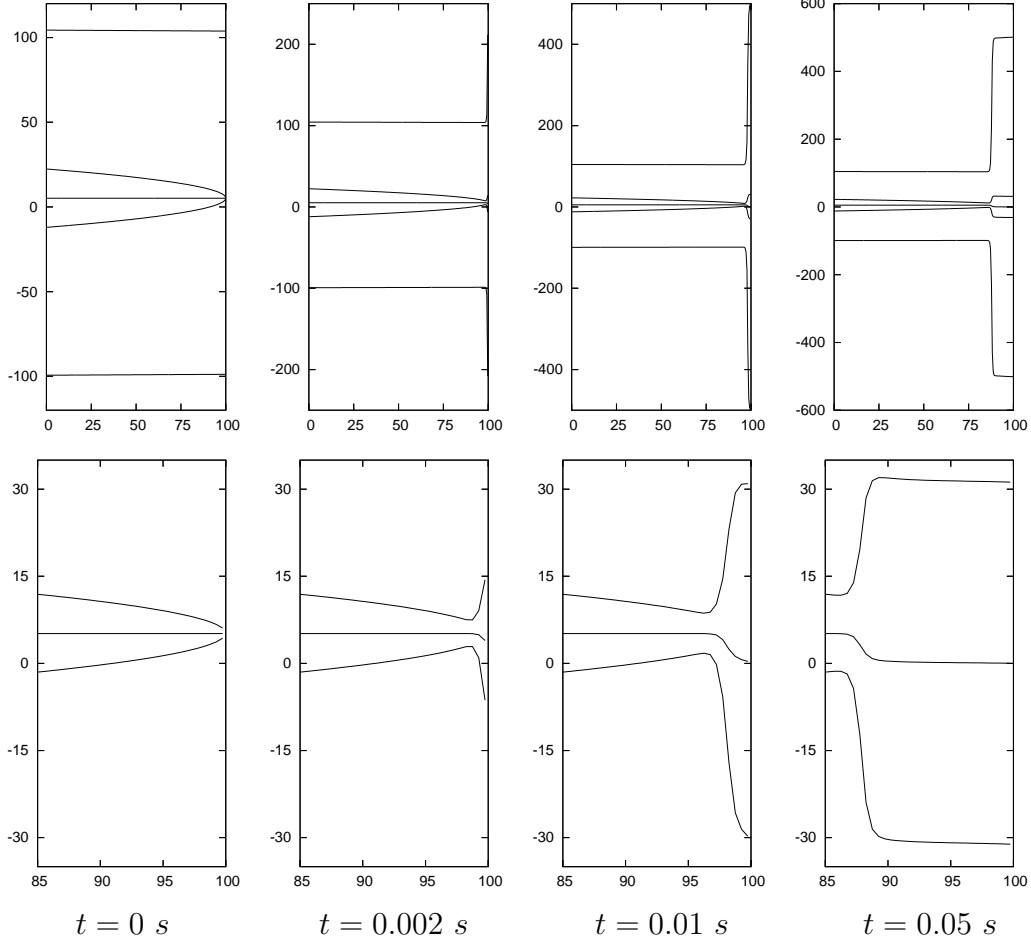
Fig. 1. Eigenvalues of matrix $\boldsymbol{C}(\boldsymbol{w}(x,t))$, $x \in (0, L = 100)$ for the simulation of the water hammer at time $t = 0$ s (steady state), $t = 0.002$ s, $t = 0.01$ s and $t = 0.05$ s, the whole computational domain (top) and the zooms around the pipe outlet (bottom)

where C_ℓ^I, C_s^I and P^I are liquid and solid fractions and pressure prescribed at the inlet and P^O is prescribed at the outlet.

- *Pipe with the closed outlet* (water hammer): numerical examples show (see Figure 1) that the number of negative values $\bar{\lambda}_l$, $l = 1, \ldots, 5$ is still equal to 3 at the inlet but 2 at the outlet (for $t \geq \eta$, $\eta \ll 1$). Accordingly, we use the boundary condition (14) at the inlet and we prescribe (zero) velocities and extrapolate fractions and pressure at the outlet , i.e. we put

$$\boldsymbol{w}(x = 0, t) = (U_\ell^{\mathrm{I-ex}}, U_s^{\mathrm{I-ex}}, C_\ell^I, C_s^I, P^I), \qquad t \in (0, T), \qquad (16)$$

$$\boldsymbol{w}(x = L, t) = (0, 0, C_\ell^{\mathrm{O-ex}}, C_s^{\mathrm{O-ex}}, P^{\mathrm{O-ex}}), \qquad t \in (0, T), \qquad (17)$$

where C_ℓ^I, C_s^I and P^I are liquid, solid fraction and pressure prescribed at the inlet.

3 Numerical methods

In this section we present several types of finite volume schemes for the solution of (7). We investigate the ability of numerical schemes to solve three following tasks:

C1 to keep a given steady state solution,
C2 to achieve a steady state solution,
C3 to simulate the unsteady water hammer.

Let $T_h = \{[x_{i-1/2}, x_{i+1/2}], \ i \in J\}$ be a partition of the computational domain $(0, L)$, where $J = \{1, 2, \ldots, M\}$ is an index set. Moreover, let $0 = t_0 < t_1 < t_2 < \ldots < t_r = T$ be a partition of the time interval $(0, T)$. We set $h_i \equiv x_{i+1/2} - x_{i-1/2}, \ i \in J$ and $\tau_k \equiv t_{k+1} - t_k$. The mean value of $\boldsymbol{w}$ over the finite volume $[x_{i-1/2}, x_{i+1/2}]$ at the time level t_k is given by

$$\boldsymbol{w}_i^k \equiv \frac{1}{h_i} \int_{x_{i-1/2}}^{x_{i+1/2}} \boldsymbol{w}(x, t_k) \, \mathrm{d}x, \quad i \in J, \ k = 0, 1, \ldots, r, \tag{18}$$

the initial state is defined by

$$\boldsymbol{w}_i^0 \equiv \frac{1}{h_i} \int_{x_{i-1/2}}^{x_{i+1/2}} \boldsymbol{w}^0(x) \, \mathrm{d}x, \quad j \in J, \tag{19}$$

where $\boldsymbol{w}^0$ is given by initial condition. Finally, let $\boldsymbol{w}_0^k, \ \boldsymbol{w}_{M+1}^k, \ k = 0, \ldots, r-1$ denote the values on "fictitious" elements obtained with the aid of boundary conditions, see Section 2.4.

3.1 Centred scheme with numerical diffusion

In [4], we used a modification of the so-called *Rusanov scheme* [3] for the solution of (7). The Rusanov scheme was used also in [21] for the simulation of two-phase flows using the two-fluid two-pressure approach. In this paper, we present the modified Rusanov scheme for the comparison with other methods. Taking, for simplicity, $h_i = h$ for all i, the scheme reads:

$$\boldsymbol{w}_i^{k+1} = \boldsymbol{w}_i^k - \frac{\tau_k}{h} \left[\boldsymbol{C}(\boldsymbol{w}_i^k)(\bar{\boldsymbol{w}}_{i+\frac{1}{2}}^k - \bar{\boldsymbol{w}}_{i-\frac{1}{2}}^k) - \frac{r_i^k}{2}(\boldsymbol{w}_{i+1}^k - 2\boldsymbol{w}_i^k + \boldsymbol{w}_{i-1}^k) - h\boldsymbol{S}_i^k \right],$$
$$i \in J, \ k = 0, 1, \ldots, r, \tag{20}$$

where

$$\bar{\boldsymbol{w}}^k_{i\pm\frac{1}{2}} = \frac{1}{2}\left(\boldsymbol{w}^k_i + \boldsymbol{w}^k_{i\pm1}\right), \qquad i \in J, \ k = 0,\ldots,r-1, \tag{21}$$

$$r^k_i = \lambda_{\max}(\boldsymbol{C}(\boldsymbol{w}^k_i)), \qquad i \in J, \ k = 0,\ldots,r-1,$$

$$\boldsymbol{S}^k_i = \boldsymbol{S}(\boldsymbol{w}^k_i), \quad k = 0,\ldots,r-1,$$

and $\lambda_{\max}(\boldsymbol{C}(\boldsymbol{w}^k_i)$ denotes the maximum absolute value of eigenvalues of matrix $\boldsymbol{C}(\boldsymbol{w}^k_i)$. The advantage of scheme (20) is that we have to calculate only the maximum eigenvalue of matrix $\boldsymbol{C}$ and do not need any other decompositions of $\boldsymbol{C}$. Consequently, the maximal eigenvalue can be computed numerically without any essential loss of accuracy.

3.2 Non-centred upwind schemes

Further, we use finite volume schemes based on approximate Riemann solvers. It is known that in presence of source terms standard methods can fail in approximating steady or nearly steady flows, see [10]. In order to ensure the approximation of steady flows, the so-called *well-balanced* schemes were presented in [25]. This approach has been extended in many papers, see, e.g., [20], [26], [27] and the references therein. Since we observed some troubles for approximating a steady state solution, we follow the approach from [25] and add to the system of equation (7) one "partial" differential equation of a known function $\sigma(x) = x$. Then we obtain the following problem

$$\frac{\partial \boldsymbol{w}}{\partial t} + \boldsymbol{C}(\boldsymbol{w})\frac{\partial \boldsymbol{w}}{\partial x} - \boldsymbol{S}(\boldsymbol{w})\frac{\partial \sigma}{\partial x} = 0, \tag{22}$$

$$\frac{\partial \sigma}{\partial t} = 0, \quad x \in (0, L), \ t \in (0, T),$$

which can be written in more compact form

$$\frac{\partial \boldsymbol{W}}{\partial t} + \boldsymbol{B}(\boldsymbol{W})\frac{\partial \boldsymbol{W}}{\partial x} = 0, \quad x \in (0, L), \ t \in (0, T), \tag{23}$$

where $\boldsymbol{W} = (\boldsymbol{w}, \sigma)^{\mathrm{T}}$ is the vector with 6 components and the block structured 6×6 matrix $\boldsymbol{B}$ is given by

$$\boldsymbol{B}(\boldsymbol{W}) = \begin{pmatrix} \boldsymbol{C}(\boldsymbol{w}) & -\boldsymbol{S}(\boldsymbol{w}) \\ 0 & 0 \end{pmatrix}. \tag{24}$$

The regular solution of problem (23) is equivalent with the solution of (7) and, moreover, system (23) is homogeneous. The eigenvalues of matrix $\boldsymbol{B}(\boldsymbol{W})$ are the eigenvalues of $\boldsymbol{C}(\boldsymbol{w})$ and, additionally, the eigenvalue zero.

Another possibility how to handle the source terms is a fractional-step method. However, numerical experiments show that by using this approach it is not possible to achieve a steady-state solution.

In the following we present several types of the so-called VFRoe-ncv ("volumes finis" Roe non-conservative variables) schemes for the numerical solution of (23). We briefly introduce an application of the VFRoe-ncv scheme for a general conservative system see e.g., [19], [20], [21] and then we describe its modifications for the non-conservative system (23). Furthermore, in Section 4 we discuss their abilities to solve problems C1 – C3.

3.2.1 VFRoe-ncv schemes for conservative system

Let us consider a general conservative hyperbolic system

$$\frac{\partial \boldsymbol{U}}{\partial t} + \frac{\partial \boldsymbol{f}(\boldsymbol{U})}{\partial x} = 0, \quad x \in (0, L), \; t \in (0, T), \tag{25}$$

where $\boldsymbol{U} : (0, L) \times (0, T) \to I\!\!R^N$ is an unknown and $\boldsymbol{f} : I\!\!R^N \to I\!\!R^N$ is a given flux. A general finite volume scheme can be written in the form

$$\boldsymbol{U}_i^{k+1} = \boldsymbol{U}_i^k - \frac{\tau_k}{h_i} \left(\boldsymbol{\Phi}_{i+1/2}^k - \boldsymbol{\Phi}_{i-1/2}^k \right), \quad i = 1, \ldots, M \tag{26}$$

where $\boldsymbol{\Phi}_{i+1/2}^k, \; i = 0, \ldots, M$ is a numerical flux through $x_{i+1/2}$ which is usually defined in the form

$$\boldsymbol{\Phi}_{i+1/2}^k \equiv \boldsymbol{\Phi}(\boldsymbol{U}_i^k, \boldsymbol{U}_{i+1}^k), \quad i = 1, \ldots, M \tag{27}$$

where $\boldsymbol{\Phi} : I\!\!R^N \times I\!\!R^N \to I\!\!R^N$ is a suitable flux function.

The basic idea of the VFRoe-ncv scheme is the following. We consider a transformation of variables $\boldsymbol{U} \to \boldsymbol{Y} = \boldsymbol{\Psi}(\boldsymbol{U})$, where $\boldsymbol{\Psi}$ is a smooth function. Although the function $\boldsymbol{\Psi}$ does not need to be necessary invertible (see [28]), for simplicity we assume that that there exists the inverse mapping $\boldsymbol{\Psi}^{-1}$. Then system (25) reads in the non-conservative form

$$\frac{\partial \boldsymbol{Y}}{\partial t} + \bar{\boldsymbol{B}}(\boldsymbol{Y}) \frac{\partial \boldsymbol{Y}}{\partial x} = 0, \quad \text{where } \bar{\boldsymbol{B}} \equiv \left(\frac{D\boldsymbol{\Psi}}{D\boldsymbol{U}} \right) \frac{D\boldsymbol{f}}{D\boldsymbol{U}} \left(\frac{D\boldsymbol{\Psi}}{D\boldsymbol{U}} \right)^{-1}. \tag{28}$$

13

Symbol $\frac{D\boldsymbol{X}}{D\boldsymbol{U}}$ denotes the Jacobian matrix of a vector-valued function $\boldsymbol{X}$. Systems (25) and (28) are equivalent for smooth solutions.

At each interface $x_{i+1/2},\ i \in J$ we solve the following linearized Riemann problem

$$\frac{\partial \boldsymbol{Y}}{\partial t} + \bar{\boldsymbol{B}}\frac{\partial \boldsymbol{Y}}{\partial x} = 0, \tag{29}$$

$$\boldsymbol{Y}(x, t = 0) = \begin{cases} \boldsymbol{Y}_L, & \text{if } x < 0, \\ \boldsymbol{Y}_R, & \text{if } x > 0, \end{cases}$$

where $\bar{\boldsymbol{B}} \equiv \boldsymbol{B}(\hat{\boldsymbol{Y}})$ and $\hat{\boldsymbol{Y}}$ is an average state depending on $\boldsymbol{Y}_L$ and $\boldsymbol{Y}_R$, and satisfying $\hat{\boldsymbol{Y}} = \boldsymbol{Y}$ if $\boldsymbol{Y}_L = \boldsymbol{Y}_R = \boldsymbol{Y}$. Obviously, we can put $\hat{\boldsymbol{Y}} = (\boldsymbol{Y}_L + \boldsymbol{Y}_R)/2$. If no eigenvalue of $\bar{\boldsymbol{B}}$ vanishes then the solution of (29) at the interface (i.e. for $\frac{x}{t} = 0$) is given by

$$\boldsymbol{Y}^*(\bar{\boldsymbol{B}}, \boldsymbol{Y}_L, \boldsymbol{Y}_R) \equiv \boldsymbol{Y}(\frac{x}{t} \to 0) = \boldsymbol{Y}_L + \sum_{\lambda_p < 0} \left(l_p^{\mathrm{T}} \cdot (\boldsymbol{Y}_R - \boldsymbol{Y}_L) \right) r_p \tag{30}$$

$$= \boldsymbol{Y}_R - \sum_{\lambda_p > 0} \left(l_p^{\mathrm{T}} \cdot (\boldsymbol{Y}_R - \boldsymbol{Y}_L) \right) r_p,$$

where $\lambda_p,\ p = 1, \ldots, N$ are real eigenvalues of $\bar{\boldsymbol{B}}$ and l_p and $r_p,\ p = 1, \ldots, N$ are the corresponding left and right eigenvectors, respectively, normalized so that $l_p \cdot r_p = 1,\ p = 1, \ldots, N$, for more detail see, e.g., [11]. Then the numerical flux in (27) is defined by

$$\boldsymbol{\Phi}(\boldsymbol{U}_L, \boldsymbol{U}_R) \equiv \boldsymbol{f}(\boldsymbol{\Psi}^{-1}(\boldsymbol{Y}^*(\bar{\boldsymbol{B}}, \boldsymbol{Y}_L, \boldsymbol{Y}_R))). \tag{31}$$

Finally, the VFRoe-ncv scheme can be written in the form

$$\boldsymbol{U}_i^{k+1} = \boldsymbol{U}_i^k - \frac{\tau_k}{h_i}\left(\boldsymbol{f}(\boldsymbol{\Psi}^{-1}(\boldsymbol{Y}_{i+1/2}^*)) - \boldsymbol{f}(\boldsymbol{\Psi}^{-1}(\boldsymbol{Y}_{i-1/2}^*)) \right), \tag{32}$$

for $i = 1, \ldots, M$, where $\boldsymbol{Y}_{i+1/2}^* \equiv \boldsymbol{Y}^*(\bar{\boldsymbol{B}}, \boldsymbol{Y}_i, \boldsymbol{Y}_{i+1}),\ i = 0, \ldots, M$ and $\boldsymbol{Y}_i \equiv \boldsymbol{\Psi}(\boldsymbol{U}_i),\ i = 0, \ldots, M + 1$.

There are some reasons why non-conservative variables $\boldsymbol{Y} = \boldsymbol{\Psi}(\boldsymbol{W})$ are used. In [19], this approach was used in order to preserve numerically Riemann invariants through the contact discontinuity. In [20], the VFRoe-ncv approach was applied to shallow-water equations with topography. Two different choices of non-conservative variables are presented there. The first one avoids troubles related with an occurrence of dry areas and the second one is suitable in order

14

to preserve all steady state solutions (not only those with a vanishing velocity). In [21], a transformation to non-conservative variables was used in order to obtain some properties of the approximate solution similar to properties of the exact solution, e.g., a positiveness of some quantities.

3.2.2 VFRoe-ncv schemes for the non-conservative system

Our aim is to apply the VFRoe-ncv scheme presented in Section 3.2.1 to the non-conservative system (23). Since one eigenvalue of $\bar{\boldsymbol{B}}$ is identically equal to zero, we define two states at the interface ($\frac{x}{t} = 0$) from left and right

$$\boldsymbol{Y}^{*,L}(\bar{\boldsymbol{B}}, \boldsymbol{Y}_L, \boldsymbol{Y}_R) \equiv \boldsymbol{Y}(\frac{x}{t} \to 0^-) = \boldsymbol{Y}_L + \sum_{\lambda_p < 0} \left(l_p^{\mathrm{T}} \cdot (\boldsymbol{Y}_R - \boldsymbol{Y}_L) \right) r_p \quad (33)$$

$$= \boldsymbol{Y}_R - \sum_{\lambda_p \geq 0} \left(l_p^{\mathrm{T}} \cdot (\boldsymbol{Y}_R - \boldsymbol{Y}_L) \right) r_p,$$

$$\boldsymbol{Y}^{*,R}(\bar{\boldsymbol{B}}, \boldsymbol{Y}_L, \boldsymbol{Y}_R) \equiv \boldsymbol{Y}(\frac{x}{t} \to 0^+) = \boldsymbol{Y}_L + \sum_{\lambda_p \leq 0} \left(l_p^{\mathrm{T}} \cdot (\boldsymbol{Y}_R - \boldsymbol{Y}_L) \right) r_p$$

$$= \boldsymbol{Y}_R - \sum_{\lambda_p > 0} \left(l_p^{\mathrm{T}} \cdot (\boldsymbol{Y}_R - \boldsymbol{Y}_L) \right) r_p.$$

Moreover, we define the averaged solution

$$\boldsymbol{Y}^{*,LR}(\bar{\boldsymbol{B}}, \boldsymbol{Y}_L, \boldsymbol{Y}_R) \equiv \frac{1}{2} \left(\boldsymbol{Y}^{*,L}(\bar{\boldsymbol{B}}, \boldsymbol{Y}_L, \boldsymbol{Y}_R) + \boldsymbol{Y}^{*,R}(\bar{\boldsymbol{B}}, \boldsymbol{Y}_L, \boldsymbol{Y}_R) \right). \quad (34)$$

We also recall a definition of the positive and negative parts of matrix $\bar{\boldsymbol{B}}$ given by

$$\bar{\boldsymbol{B}}^{\pm} \equiv \boldsymbol{R} \mathrm{Diag}(\lambda_1^{\pm}, \ldots, \lambda_6^{\pm}) \boldsymbol{L}^{\mathrm{T}}, \quad (35)$$

where $\boldsymbol{L}$ and $\boldsymbol{R}$ are matrices whose columns are the left and right eigenvectors of $\bar{\boldsymbol{B}}$, respectively, $\mathrm{Diag}(\lambda_1^{\pm}, \ldots, \lambda_6^{\pm})$ is a diagonal matrix, where λ_i, $i = 1, \ldots, 6$ are eigenvalues of $\bar{\boldsymbol{B}}$ and $a^+ = \max(a, 0)$, $a^- = \min(a, 0)$.

It is possible to observe that the solutions of the local Riemann problem satisfy the relations

$$\bar{\boldsymbol{B}} \boldsymbol{Y}^{*,L}(\bar{\boldsymbol{B}}, \boldsymbol{Y}_L, \boldsymbol{Y}_R) = \bar{\boldsymbol{B}} \boldsymbol{Y}^{*,R}(\bar{\boldsymbol{B}}, \boldsymbol{Y}_L, \boldsymbol{Y}_R) = \bar{\boldsymbol{B}} \boldsymbol{Y}^{*,LR}(\bar{\boldsymbol{B}}, \boldsymbol{Y}_L, \boldsymbol{Y}_R)$$

$$= \bar{\boldsymbol{B}} \boldsymbol{Y}_R - \bar{\boldsymbol{B}}^+ (\boldsymbol{Y}_R - \boldsymbol{Y}_L) = \bar{\boldsymbol{B}} \boldsymbol{Y}_L - \bar{\boldsymbol{B}}^- (\boldsymbol{Y}_R - \boldsymbol{Y}_L). \quad (36)$$

In case that $\bar{\boldsymbol{B}}$ is a regular matrix the previous relations imply that

$$\boldsymbol{Y}^{*,L}(\bar{\boldsymbol{B}}, \boldsymbol{Y}_L, \boldsymbol{Y}_R) = \boldsymbol{Y}^{*,R}(\bar{\boldsymbol{B}}, \boldsymbol{Y}_L, \boldsymbol{Y}_R),$$

15

which is in agreement with the existence of a unique solution of the linearized Riemann problem at $\frac{x}{t} = 0$ for $\bar{\boldsymbol{B}}$ having no vanishing eigenvalues.

We will use $\boldsymbol{Y} \equiv \boldsymbol{W}$ in (28). It would be possible to consider different (non-conservative) variables. However, as the matrix $\boldsymbol{B}(\boldsymbol{W})$ is defined by rather complicated relations the choice of other variables than the mentioned one will probably still increase the complexity of the problem. From the point of view that the transformation of variables is the identity ($\boldsymbol{\Psi} \equiv$ identity) the following schemes can be called as the VFRoe scheme. However, since the components of $\boldsymbol{W}$ are non-conservative we still use the notation "VFRoe-ncv scheme".

In the following, we set $\boldsymbol{W}_i^k \equiv (\boldsymbol{w}_i^k, x_i)^{\mathrm{T}}$, $i = 0, \ldots, M + 1$, $k = 0, \ldots, r - 1$, where x_i is the centre of interval $[x_{i-1/2}, x_{i+1/2}]$, $i = 1, \ldots, M$ and $x_0 = 2x_{1/2} - x_1$, $x_{M+1} = 2x_{M+1/2} - x_M$, which denote discrete values of $\boldsymbol{W}$ on the "fictitious" elements. It means that we put $\sigma_L = x_{i-1}$ and $\sigma_R = x_i$ for the Riemann problem considered at the face localized at $x_{i+1/2}$. This choice has no influence on the solution of the Riemann problem, e.g., the choice $\sigma_L = \sigma_R = x_{i+1/2}$ produces very similar results for the "physical" components of the solution.

Provided that we formally replace $\boldsymbol{f}(\boldsymbol{U})$ by $\boldsymbol{B}(\boldsymbol{U})\boldsymbol{U}$ in (32) and take into account that $\boldsymbol{\Psi}$ is the identity, we obtain the following form of the VFRoe-ncv scheme for the non-conservative system (23) (with no vanishing eigenvalues)

$$\boldsymbol{W}_i^{k+1} = \boldsymbol{W}_i^k - \frac{\tau_k}{h_i} \left[\boldsymbol{B}(\boldsymbol{W}_{i+\frac{1}{2}}^{k,*}) \boldsymbol{W}_{i+\frac{1}{2}}^{k,*} - \boldsymbol{B}(\boldsymbol{W}_{i-\frac{1}{2}}^{k,*}) \boldsymbol{W}_{i-\frac{1}{2}}^{k,*} \right], \qquad (37)$$

for $i \in J$, $k = 0, \ldots, r - 1$, where vectors $\boldsymbol{W}_{i+\frac{1}{2}}^{k,*}$, $i = 0, \ldots, M$, $k = 0, 1, \ldots, r$ are the solutions of the local Riemann problems.

Another possibility is to replace the arguments of the matrix $\boldsymbol{B}(\cdot)$ in (37) by the volume mean of $\boldsymbol{W}$ on $[x_{i-1/2}, x_{i+1/2}]$, then we have

$$\boldsymbol{W}_i^{k+1} = \boldsymbol{W}_i^k - \frac{\tau_k}{h_i} \left[\boldsymbol{B}(\boldsymbol{W}_i^k) \left(\boldsymbol{W}_{i+\frac{1}{2}}^{k,*} - \boldsymbol{W}_{i-\frac{1}{2}}^{k,*} \right) \right]. \qquad (38)$$

Further, we can modify the scheme (38) by

$$\boldsymbol{W}_i^{k+1} = \boldsymbol{W}_i^k - \frac{\tau_k}{h_i} \left[\boldsymbol{B} \left(\frac{1}{2} (\boldsymbol{W}_{i+\frac{1}{2}}^{k,*} + \boldsymbol{W}_{i-\frac{1}{2}}^{k,*}) \right) \left(\boldsymbol{W}_{i+\frac{1}{2}}^{k,*} - \boldsymbol{W}_{i-\frac{1}{2}}^{k,*} \right) \right] \qquad (39)$$

or by

$$\boldsymbol{W}_i^{k+1} = \boldsymbol{W}_i^k - \frac{\tau_k}{h_i} \left[\frac{1}{2} \left(\boldsymbol{B}(\boldsymbol{W}_{i+\frac{1}{2}}^{k,*}) + \boldsymbol{B}(\boldsymbol{W}_{i-\frac{1}{2}}^{k,*}) \right) \left(\boldsymbol{W}_{i+\frac{1}{2}}^{k,*} - \boldsymbol{W}_{i-\frac{1}{2}}^{k,*} \right) \right]. \qquad (40)$$

16

All four variants of the VFRoe-ncv schemes (37) – (40) are identical for a linear system of hyperbolic equations (i.e., if $\boldsymbol{B}$ is constant) and are well-defined. The schemes were defined rather heuristically and some numerical analysis should be carried out. Unfortunately, the complexity of the model does not allow us to derive analytically some properties of the matrix $\boldsymbol{B}$ and therefore to analyse the schemes (37) – (40). On the other hand we suppose that a numerical analysis carried out for some simplified problem will produce results which will not correspond to the original model. However, our aim is not to derive and to analyse the VFRoe-ncv scheme for a general non-conservative system but to show that these variants of the VFRoe-ncv scheme (using the solution of a linearized Riemann problem) can not be used for flow simulation of solid-liquid-gas slurries with the virtual mass effect (at least for the configurations studied in this paper). An application of VFRoe-ncv schemes to another non-conservative problem is quite open. In [21] the VFRoe-ncv scheme of type (40) was applied for a discretization of non-conservative terms in a modelling of two-phase flows using two-fluid two-pressure approach.

Since one eigenvalue of $\boldsymbol{B}$ in (23) is identically equal to zero, we have two possible solutions of the linearized Riemann problem and therefore with the aid of (33) – (34) we define more variants of VFRoe-ncv schemes for (23). Let $\boldsymbol{B}_{i+1/2}^{k} \equiv \boldsymbol{B}((\boldsymbol{W}_i^k + \boldsymbol{W}_{i+1}^k)/2)$, $i = 0, \ldots, M$, $k = 0, \ldots, r-1$ and

$$\boldsymbol{W}_{i+\frac{1}{2}}^{k,*,L} = \boldsymbol{Y}^{*,L}(\boldsymbol{B}_{i+1/2}^k, \boldsymbol{W}_i^k, \boldsymbol{W}_{i+1}^k), \tag{41}$$
$$\boldsymbol{W}_{i+\frac{1}{2}}^{k,*,R} = \boldsymbol{Y}^{*,R}(\boldsymbol{B}_{i+1/2}^k, \boldsymbol{W}_i^k, \boldsymbol{W}_{i+1}^k),$$
$$\boldsymbol{W}_{i+\frac{1}{2}}^{k,*,LR} = \boldsymbol{Y}^{*,LR}(\boldsymbol{B}_{i+1/2}^k, \boldsymbol{W}_i^k, \boldsymbol{W}_{i+1}^k),$$

where $i = 0, \ldots, M$, $k = 0, \ldots, r-1$. Based on (40) we define the first variant of the *VFRoe-ncv scheme* by

$$\boldsymbol{W}_i^{k+1} = \boldsymbol{W}_i^k - \frac{\tau_k}{h_i} \left[\frac{1}{2} \left(\boldsymbol{B}(\boldsymbol{W}_{i+\frac{1}{2}}^{k,*,L}) + \boldsymbol{B}(\boldsymbol{W}_{i-\frac{1}{2}}^{k,*,R}) \right) \right. \tag{42}$$
$$\left. \left(\boldsymbol{W}_{i+\frac{1}{2}}^{k,*,L} - \boldsymbol{W}_{i-\frac{1}{2}}^{k,*,R} \right) \right],$$

and the second one by

$$\boldsymbol{W}_i^{k+1} = \boldsymbol{W}_i^k - \frac{\tau_k}{h_i} \left[\frac{1}{2} \left(\boldsymbol{B}(\boldsymbol{W}_{i+\frac{1}{2}}^{k,*,LR}) + \boldsymbol{B}(\boldsymbol{W}_{i-\frac{1}{2}}^{k,*,LR}) \right) \right. \tag{43}$$
$$\left. \left(\boldsymbol{W}_{i+\frac{1}{2}}^{k,*,LR} - \boldsymbol{W}_{i-\frac{1}{2}}^{k,*,LR} \right) \right],$$

where $i \in J$, $k = 0, \ldots, r-1$.

Based on (38) we introduce two variants of the *simplified VFRoe-ncv scheme,* the first one by

$$\boldsymbol{W}_i^{k+1} = \boldsymbol{W}_i^k - \frac{\tau_k}{h_i}\left[\boldsymbol{B}(\boldsymbol{W}_i^k)\left(\boldsymbol{W}_{i+\frac{1}{2}}^{k,*,L} - \boldsymbol{W}_{i-\frac{1}{2}}^{k,*,R}\right)\right], \tag{44}$$

and the second by

$$\boldsymbol{W}_i^{k+1} = \boldsymbol{W}_i^k - \frac{\tau_k}{h_i}\left[\boldsymbol{B}(\boldsymbol{W}_i^k)\left(\boldsymbol{W}_{i+\frac{1}{2}}^{k,*,LR} - \boldsymbol{W}_{i-\frac{1}{2}}^{k,*,LR}\right)\right], \tag{45}$$

where again $i \in J$, $k = 0, \ldots, r-1$. It would be possible to define additional numerical schemes based on (37) and (39) of course, but computational experiments show that the numerical results obtained by these variants behave very similarly as the schemes (42) and (43), see [5]. That is why we do not introduce them.

On the other hand, we define a scheme which is a direct generalization of the pure upwind scheme for a linear system of equations. Let $\boldsymbol{B}_{i+\frac{1}{2}}^{k,\pm}$ be the positive and negative parts of $\boldsymbol{B}_{i+\frac{1}{2}}^k = \boldsymbol{B}((\boldsymbol{W}_i^k + \boldsymbol{W}_{i+1}^k)/2)$, $i = 0, \ldots, M$, $k = 0, \ldots, r-1$ given by (35). Then we define the *generalized upwind scheme*

$$\boldsymbol{W}_i^{k+1} = \boldsymbol{W}_i^k - \frac{\tau_k}{h_i}\left[\boldsymbol{B}_{i+\frac{1}{2}}^{k,-}\left(\boldsymbol{W}_{i+1}^k - \boldsymbol{W}_i^k\right) + \boldsymbol{B}_{i-\frac{1}{2}}^{k,+}\left(\boldsymbol{W}_i^k - \boldsymbol{W}_{i-1}^k\right)\right], \tag{46}$$

where $i \in J$, $k = 0, \ldots, r-1$. With the aid of (36), scheme (46) can be rewritten in the equivalent form as

$$\boldsymbol{W}_i^{k+1} = \boldsymbol{W}_i^k - \frac{\tau_k}{h_i}\left[\boldsymbol{B}_{i+\frac{1}{2}}^k\left(\boldsymbol{W}_i^k - \boldsymbol{W}_{i+\frac{1}{2}}^{k,*,P}\right) - \boldsymbol{B}_{i-\frac{1}{2}}^k\left(\boldsymbol{W}_{i-\frac{1}{2}}^{k,*,P} - \boldsymbol{W}_i^k\right)\right], \tag{47}$$

where ^{k,*,P} represents either ^{k,*,L} or ^{k,*,R} or ^{k,*,LR}. The scheme (47) is the scheme of Chakravarthy et al. presented in [29]. Although the schemes (46) and (47) are analytically identical the numerical examples in Section 4 show that their implementations produce rather different numerical solutions.

We have introduced six non-centred numerical schemes (42) – (47) for the solution of (23). If $\boldsymbol{B}$ is a regular constant matrix (i.e. system (23) is linear) then with the aid of (36) we observe that all these schemes are identical. In order to guarantee the stability of these schemes we use the *stability condition*

$$\tau_k \leq \text{CFL} \min\left(\min_{i=1,\ldots,M} \frac{h_i}{\lambda_{\max}\left(\boldsymbol{B}(\boldsymbol{W}_i^k)\right)}, \min_{\substack{i=1,\ldots,M-1 \\ P=L,R}} \frac{(h_i + h_{i+1})/2}{\lambda_{\max}\left(\boldsymbol{B}(\boldsymbol{W}_{i+\frac{1}{2}}^{k,*,P})\right)}\right), \tag{48}$$

18

where $k = 0, \ldots, r - 1$ and CFL $\in (0, 1)$.

4 Numerical examples

4.1 Problem data

In this section we discuss the ability of schemes (20), (42) – (47) to solve the tasks C1 – C3 introduced in Section 3. Using data from [2] the calculations were carried out with the following values of the model parameters in (3) – (5) corresponding to a sand (solid), water (liquid) and air (gas): $\rho_s = 2600 \ kg.m^{-3}$, $\rho_l = 1000 \ kg.m^{-3}$, $\rho_g = 1.28 \ kg.m^{-3}$, $a_s = 7000 \ m.s^{-1}$, $a_l = 500 \ m.s^{-1}$, $a_g = 300 \ m.s^{-1}$, $f_\ell = 0.04$, $D = 0.1m$, $C_D = 0.1$, $d = 5.10^{-4}m$, $\frac{dz}{dx} = 0$ and the length of the pipe is $L = 100 \ m$. Moreover, the following initial and boundary conditions were used for the tasks C1 – C3 defined at the beginning of Section 3:

C1 We use the boundary conditions (14) – (15) with $C_\ell^I = 0.89$, $C_s^I = 0.1$, $P^I = 5.5 \cdot 10^5 \ Pa$ and $P^O = 0 \ Pa$. The initial condition is defined by the steady state solution

$$\boldsymbol{w}_0 = \boldsymbol{w}^{\text{steady}} \equiv (5.049, \ 5.219, \ 0.89, \ 0.1, \ 5.5 \cdot 10^5(1 - x/L)), \tag{49}$$

which corresponds to the mentioned boundary conditions. It was computed numerically but can be easily verified analytically. We investigate the ability of the schemes to keep the steady state solution (49) for $t \to \infty$.

C2 We use the same boundary conditions as in C1 and the initial condition

$$\boldsymbol{w}_0 = (6.5, \ 6.5, \ 0.89, \ 0.1, \ 5.5 \cdot 10^5(1 - x/L)). \tag{50}$$

We investigate the ability of the schemes to converge to the steady state solution (49) for $t \to \infty$.

C3 We investigate the ability of the schemes to simulate the unsteady water hammer. We use the boundary conditions (16) – (17) with $C_\ell^I = 0.89$, $C_s^I = 0.1$, $P^I = 5.5 \cdot 10^5 \ Pa$ and the (steady state) initial condition (49). We compute the solution for time interval $(0, 0.3) \ s$ during whose the water hammer propagates up to the pipe inlet.

The comparison of the numerical methods were performed mostly for 25 subintervals of $(0, L)$ ($M = 25$), some calculations on finer meshes are presented.

19

Based on many numerical experiments, the following interesting but unpleasant property of the linearized Riemann solutions (33) – (34) was observed. By $\boldsymbol{W} = (\boldsymbol{w}, \sigma)^{\mathrm{T}} \in \mathrm{PAS}$ we mean that $\boldsymbol{w} \in \mathrm{PAS}$, see (6). There exist vectors $\boldsymbol{W}_L \in \mathrm{PAS}$ and $\boldsymbol{W}_R \in \mathrm{PAS}$ such that

$$\boldsymbol{Y}^{*,P}(\boldsymbol{B}((\boldsymbol{W}_L + \boldsymbol{W}_R)/2), \boldsymbol{W}_L, \boldsymbol{W}_R) \notin \mathrm{PAS}, \tag{51}$$

where $\boldsymbol{Y}^{*,P}$ represents either $\boldsymbol{Y}^{*,L}$ or $\boldsymbol{Y}^{*,R}$ or $\boldsymbol{Y}^{*,LR}$. This property was observed in regions of the computational domain $(0, L)$, where one (not identically vanishing) eigenvalue of $\boldsymbol{B}((\boldsymbol{W}_L + \boldsymbol{W}_R)/2)$ is close to zero. The matrix $\boldsymbol{B}$ contains one eigenvalue identically equal to zero (vanishing eigenvalue) but it does not cause any troubles in computations.

The property (51) is documented in Table 1, where examples of the solutions $\boldsymbol{Y}^{*,L}$ and $\boldsymbol{Y}^{*,R}$ of the linearized Riemann problem (29) for four pairs of vectors $\boldsymbol{W}_L$ and $\boldsymbol{W}_R$ are shown. The nonphysical quantities are bolted and the table also contains the corresponding eigenvalues λ_i, $i = 1, \ldots, 6$ of the matrix $\boldsymbol{B}((\boldsymbol{W}_L + \boldsymbol{W}_R)/2)$. The physical inadmissibility of $\boldsymbol{Y}^{*,L}$ and $\boldsymbol{Y}^{*,R}$ is probably the main reason of the disability of the schemes using the solution of the linearized Riemann problem to solved satisfactory the tasks C1 – C3. The fact that the solution of the linearized Riemann problem can be unphysical may depend on the choice of the variable for the linearization process in VFRoencv, see [30]. But for the considered model, as we mentioned in Section 3.2.2, we do not know what natural choice (better than the used one) of the variables for the linearization process could be done. The nonphysical solutions of the linearized Riemann problem appear also for conservative systems, see, e.g, [31] where the vacuum scenario of the Euler equations is investigated. We suppose that the situation from [31] differs from those ones presented in Table 1 since the velocity directions are completely different.

In the following, we discuss the obtained numerical results for each group of the schemes separately.

Modified Rusanov scheme   The modified Rusanov scheme (20) gives satisfactory numerical results for all three tasks. It keeps the steady state solution in the task C1 and the solution of the task C2 do not suffer from any unphysical oscillations. Finally, Figure 2 shows the simulation of the water hammer. We observe that the Rusanov scheme yields to a slower propagation of changes of the state vector for the water hammer in comparison with other schemes, compare Figures 2 and 6.

example		$\boldsymbol{W}_L$	$\boldsymbol{W}_R$	$\boldsymbol{Y}^{*,L}$	$\boldsymbol{Y}^{*,R}$	$\lambda_1, \ldots, \lambda_6$
E1	U_ℓ	6.500	6.500	4.457	6.401	104.7
	U_s	6.500	6.500	17.223	6.820	-98.2
	C_ℓ	0.890	0.890	**1.052**	0.885	13.4
	C_s	0.100	0.100	**-0.055**	0.1050	6.5
	P	93500.	82500.	85624.	79369	-0.43
	σ	83.	85.	83.	85.	0.
E2	U_ℓ	6.616	6.690	-9.940	4.499	105.3
	U_s	5.670	4.930	80.672	19.093	-98.2
	C_ℓ	0.890	0.890	**1.906**	0.705	13.2
	C_s	0.100	0.100	**-0.882**	0.280	6.0
	P	115917.	105766	67914	126308	-2.3
	σ	79.	81.	79.	81.	0.
E3	U_ℓ	6.963	7.259	-147.844	-11.931	107.1
	U_s	3.177	0.221	477.934	302.555	-98.3
	C_ℓ	0.890	0.890	**7.638**	**-2.744**	9.8
	C_s	0.100	0.100	**-6.466**	**3.872**	-5.5
	P	117170	109562	655575	791811	4.0
	σ	79.	81.	79.	81.	0.
E4	U_ℓ	3.563	0.	6.651	27.828	14.991
	U_s	4.317	0.	-13.841	19.019	-6.480
	C_ℓ	0.899	0.899	0.7282	**250.115**	3.9
	C_s	0.102	0.102	0.272	**1.692**	0.2
	P	214037	214037	250072	**-6.15E+10**	0.2
	σ	98.	102.	98.	102.	0.

Table 1

Examples of solutions $\boldsymbol{Y}^{*,L}$ and $\boldsymbol{Y}^{*,R}$ of the linearized Riemann problem for four pairs of $\boldsymbol{Y}_L$ and $\boldsymbol{Y}_R$ and the corresponding eigenvalues λ_i, $i = 1, \ldots, 6$, physically inadmissible quantities are bolted

VFRoe-ncv schemes (42) and (43) Scheme (43) is not able to solve the task C1 what is documented in Figure 3, where the dependence of the velocities U_ℓ and U_s at the cell with $x_i = 91$ on the number of time steps is presented. We observe that after approximately 50 time steps some instabilities of the numerical solution arise and consequently the solution blows up very fastly. This instability is not caused by a violation of a stability condition with respect to the length of the time step (the presented results were obtained with CFL = 0.005 in (48)) but we suppose that these instabilities come from a very high sensitivity of the solution of the Riemann problem with respect to rounding errors. It make no sense in applying the schemes (43) to the tasks C2 and C3.

Scheme (42) is able to solve the task C1 but not the task C2. The failures of the scheme is caused by the property (51) since $\boldsymbol{B}(\boldsymbol{W}_{i+\frac{1}{2}}^{k,*,P})$ becomes meaningless for $\boldsymbol{W}_{i+\frac{1}{2}}^{k,*,P} \notin$ PAS. Here ^{*,P} represent ^{*,L} or ^{*,R} or ^{*,LR} and i corresponds to the finite volume with the unphysical state vector. The example E1 in Table
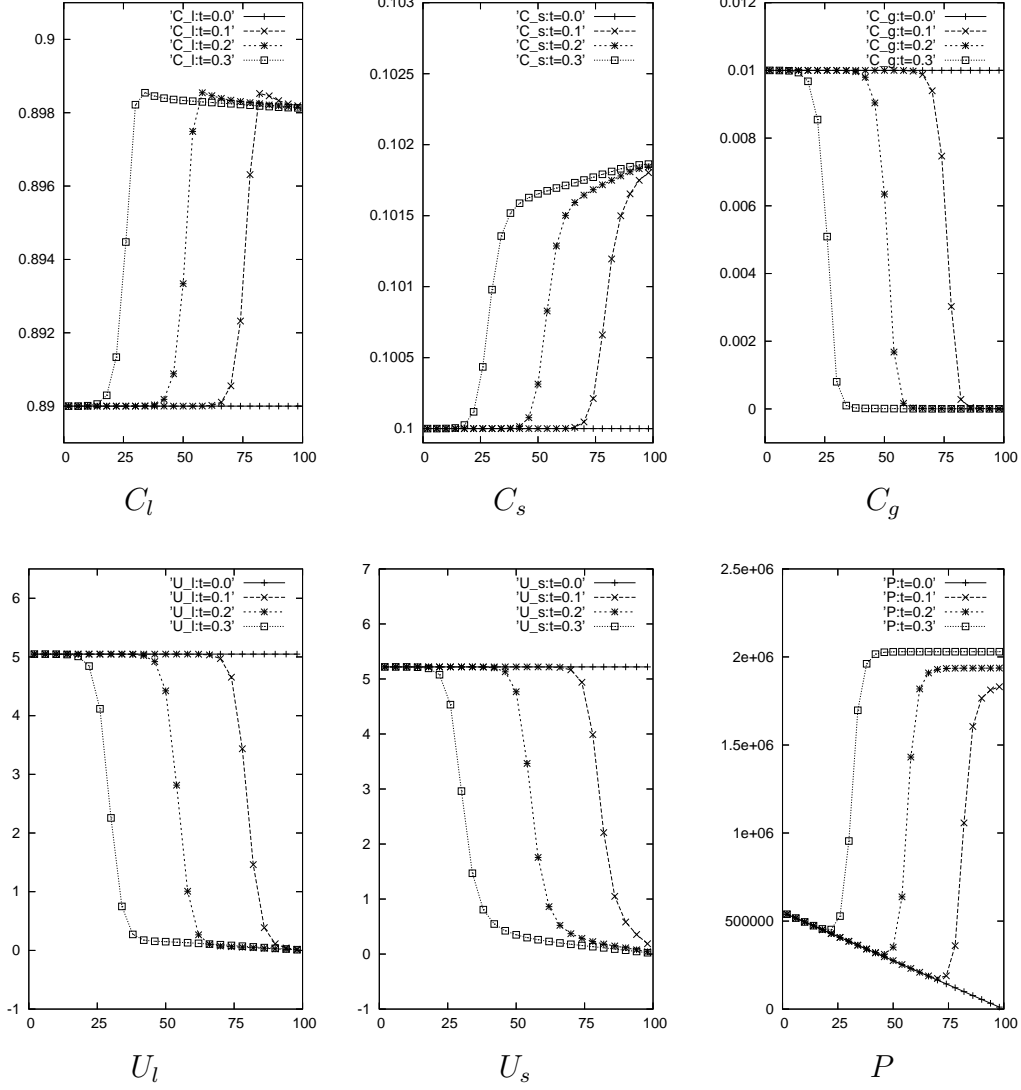
21

Fig. 2. Task C3, $M = 25$, modified Rusanov scheme (20), simulation of the water hammer, distributions of C_ℓ, C_s, C_g, U_ℓ, U_s and P at $t = 0$, $t = 0.1$, $t = 0.2$ and $t = 0.3$

1 corresponds to the application of the scheme (43) to the task C2. It make no sense in applying the scheme (43) to the task C3.

Simplified VFRoe-ncv schemes Schemes (44) – (45) give significantly better results than schemes (42) – (43). It is caused by the fact that solutions of linearized Riemann problems are not used as arguments of matrix $\boldsymbol{B}$ but they appear in (44) and (45) only as differences $\boldsymbol{W}^{k,*,L}_{i+\frac{1}{2}} - \boldsymbol{W}^{k,*,R}_{i-\frac{1}{2}}$ and $\boldsymbol{W}^{k,*,LR}_{i+\frac{1}{2}} - \boldsymbol{W}^{k,*,LR}_{i-\frac{1}{2}}$, respectively. We observed the following situation

$$\boldsymbol{W}^{k,*,L}_{i+\frac{1}{2}} \notin \text{PAS} \text{ and } \boldsymbol{W}^{k,*,R}_{i-\frac{1}{2}} \notin \text{PAS}, \text{ but } (\boldsymbol{W}^{k,*,L}_{i+\frac{1}{2}} - \boldsymbol{W}^{k,*,R}_{i-\frac{1}{2}}) \in \text{PAS}, \quad (52)$$
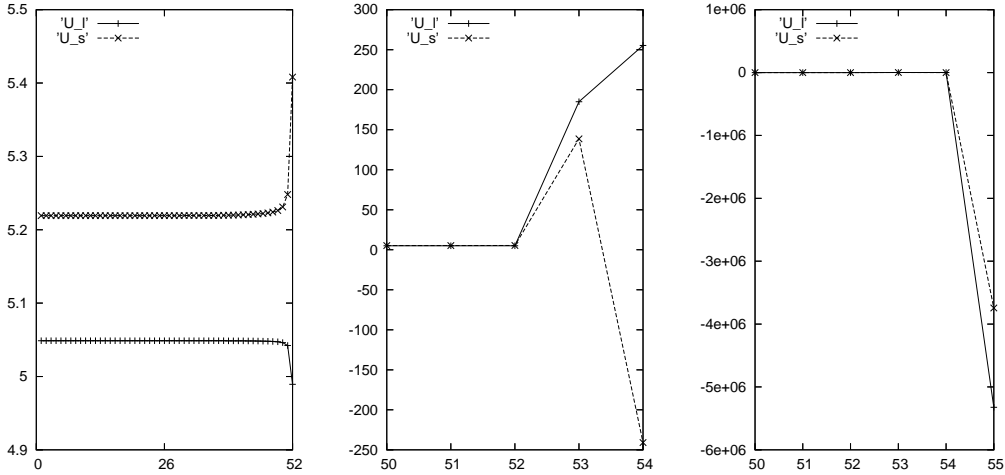
Fig. 3. Task C1, $M = 50$, VFRoe-ncv scheme (43), dependence of U_ℓ and U_s at the cell with $x_i = 91$ on the number of time steps

which causes trouble for scheme (42) but not for (44). This explains the better behaviour of (44) – (45) compared to (42) – (43).

The scheme (45) solves well the tasks C1 and C2. The scheme (44) solves well the task C1, but for the task C2 it converges to an unphysical "steady state" solution containing spurious oscillations, which are localized near a node where a non-vanishing eigenvalue is close to zero, see Figure 4. It is interesting that these oscillations are completely independent of the value of CFL number used in the stability condition (48)) and the oscillating solution represents a steady state solution form the numerical point of view, i.e., there exists $k_0 > 0$ such that $\boldsymbol{w}_i^{k+1} = \boldsymbol{w}_i^k$, $i = 1, \ldots, M$ for any $k \geq k_0$.

On the other hand, both schemes (44) – (45) are able to solve the task C3, but the solutions suffer from instabilities near the pipe outlet, where one non-vanishing eigenvalue is small. These instabilities are stronger for the scheme (44) and can not be suppressed by reducing the time step. Figure 5 shows the simulation of the water hammer obtained by the scheme (44), where the instabilities are observed.

Generalized upwind schemes Although schemes (46) and (47) are analytically identical they give numerically identical results only for tasks C1 and C2. They solve very well C1 but for C2 converge to an unphysical steady state solution, similarly as scheme (44), see Figure 4.

However, schemes (46) – (47) are also able to solve the unsteady problem C3. Using (46) we obtain a very good simulation of the water hammer for the similar CFL number (CFL = 0.3) as the modified Rusanov scheme (20), see Figure 6. On the other hand with the aid of scheme (47) the calculation
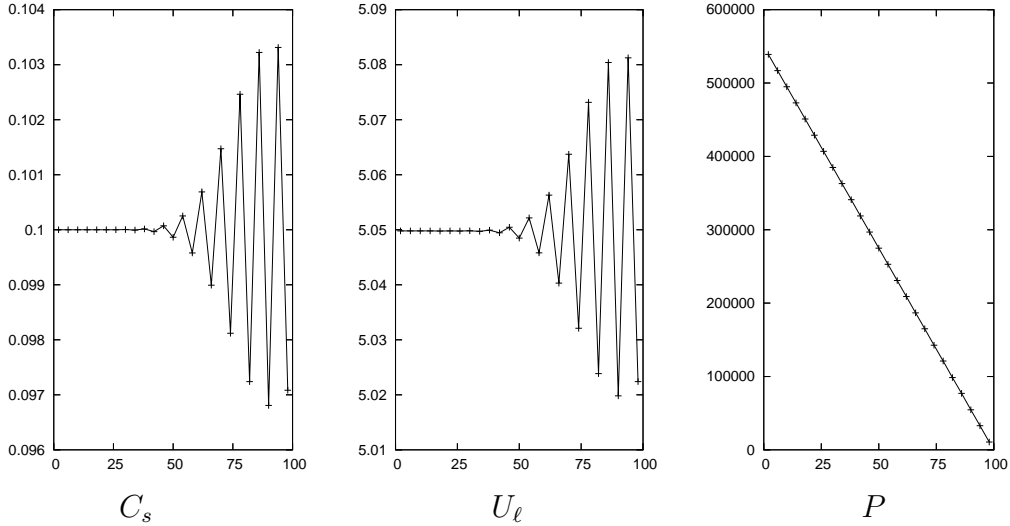
23

Fig. 4. Task C2, $M = 25$, simplified VFRoe-ncv scheme (44), unphysical "steady state" solution, distributions of C_s, U_ℓ, and P
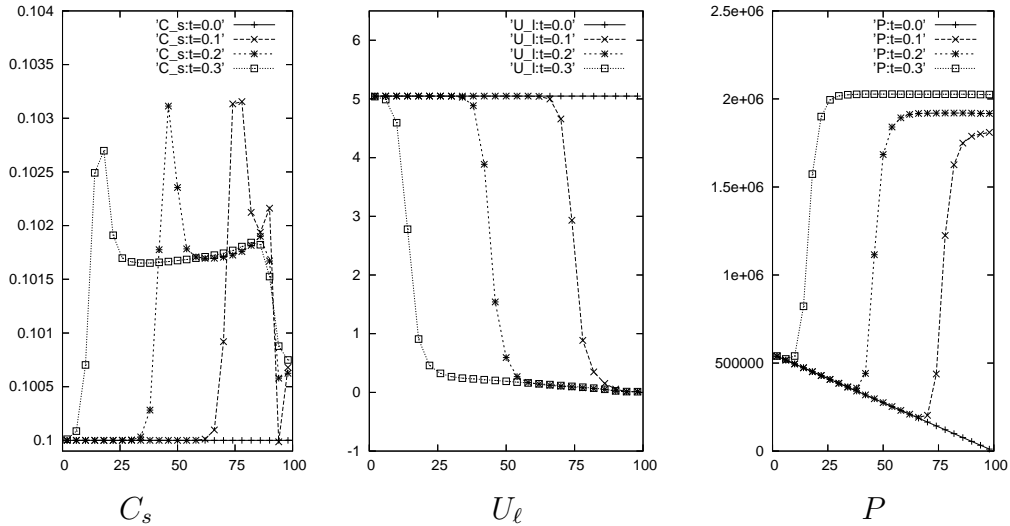

Fig. 5. Task C3, $M = 25$, simplified VFRoe-ncv scheme (44), simulation of the water hammer, distributions of C_s, U_ℓ and P at $t = 0$, $t = 0.1$, $t = 0.2$ and $t = 0.3$

can be carried out successfully only if CFL ≤ 0.2 in (48)). This is a very important observation that two analytically identical schemes have different computational properties. This is caused probably by the fact that the scheme (47) uses the solution of linearized Riemann problems whose computation is more sensitive with respect to the rounding errors. Therefore smaller time step should be used in order to avoid instabilities caused probably by rounding errors. The example E4 from Table 1 corresponds to the solution of the water hammer obtained by the scheme (47) with CFL $= 0.29$ in the third time step. We observe that the solution of the linearized Riemann problem at $x = 100$ (the pipe outlet) is very unphysical $P \ll 0$. On the other hand, using the numerical solution obtained by the scheme (47) with CFL $= 0.29$ after
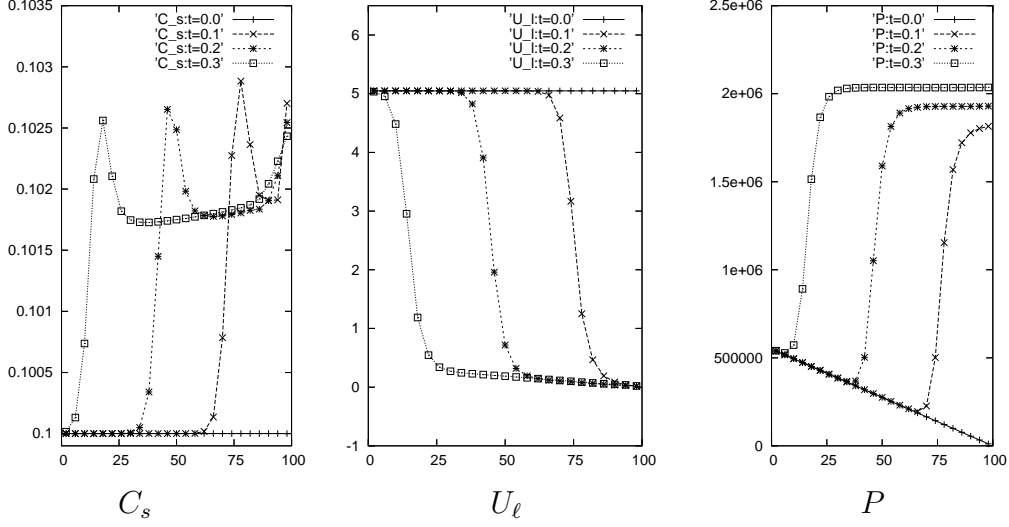
24

Fig. 6. Task C3, $M = 25$, generalized upwind scheme (46), simulation of the water hammer, distributions of C_s, U_ℓ and P at $t = 0$, $t = 0.1$, $t = 0.2$ and $t = 0.3$

	Computational task		
method	C1	C2	C3
Rusanov (20)	OK	OK	OK
VFRoe-ncv1 (42)	OK	fails	–
VFRoe-ncv2 (43)	fails	fails	–
VFRoe-ncv-sim1 (44)	OK	OK stable oscillations	OK unstable oscillations
VFRoe-ncv-sim2 (45)	OK	OK	OK unstable oscillations
upwind1 (46)	OK	OK stable oscillations	OK if CFL ≤ 0.3
upwind2 (47)	OK	OK stable oscillations	OK if CFL ≤ 0.2

Table 2
Properties of numerical schemes (20), (42) – (47)

two time steps as an initial condition for the scheme (46) we obtain results practically identical with those presented in Figure 6. Based (not only) on this observation we suppose that *numerical schemes* based on the solution of the *linearized Riemann problem* are *not suitable* for a flow simulation of solid-liquid-gas slurries.

4.3 Summary of the results

The properties of the numerical schemes (20), (42) – (47) observed in Section 4.2 are summarised in Table 2. The numerical examples presented in Section 4.2 indicate that none of the numerical schemes (42) – (47) is able to solve the tasks C1 – C3. The best results were obtained by scheme (46) whose simulation of the water hammer looks realistic and CFL number in (48)) is not too restrictive. The only drawback of (46) is that it converges to an unphysical steady state solution for the task C2. This lack can be overcome by adding a small dissipative term to the scheme, e.g.,

$$\boldsymbol{W}_i^{k+1} = \boldsymbol{W}_i^k - \frac{\tau_k}{h_i} \left[\boldsymbol{B}_{i+\frac{1}{2}}^{k,-} \left(\boldsymbol{W}_{i+1}^k - \boldsymbol{W}_i^k \right) + \boldsymbol{B}_{i-\frac{1}{2}}^{k,+} \left(\boldsymbol{W}_i^k - \boldsymbol{W}_{i-1}^k \right) \right. \tag{53}$$
$$\left. -\epsilon \frac{r_i^k}{2} (\boldsymbol{W}_{i+1}^k - 2\boldsymbol{W}_i^k + \boldsymbol{W}_{i-1}^k) \right], \quad i \in J, \ k = 0, \ldots, r - 1,$$

where $\epsilon > 0$. Numerical examples show that the value of $\epsilon \geq 0.01$ ensures that numerical solution of the task C2 converges to a physical steady state (49). On the other hand, the presence of artificial viscosity causes a retarding and a small smearing of the solution for the task C3. Figure 7 compares simulations of the water hammer obtained by the Rusanov scheme (20) and scheme (53) with $\epsilon = 1$, $\epsilon = 0.1$ and $\epsilon = 0.01$ (= scheme (46)) with $M = 50$, $M = 200$ and $M = 800$, respectively (for $\epsilon \leq 0.01$ the results are almost identical with the results obtained with $\epsilon = 0$). We observe an increase of the retardation for propagation of discontinuities for increasing ϵ. Moreover, this figure shows that with the aid of a finer partitioning of $(0, L)$ we obtain a sharper capturing of discontinuities but the same retardation for each numerical scheme.

Therefore, we conclude that the Rusanov scheme and the schemes (53) with different parameter ϵ converge to different "weak" solutions (differing by the speed of the propagation of the discontinuities). This is in agreement with the arguments presented in the introduction and Remark 2 of this paper, i.e., without additional (jump) conditions we can not define a proper weak solution and then different stable numerical schemes produce different solutions.

5 Conclusion

We dealt with the numerical simulation of steady and unsteady flows of solid-liquid-gas slurries which leads to a non-conservative system of equations with source terms. Although the non-conservativity and complexity of the problems prevented us from introducing the concept of a weak solution we solved
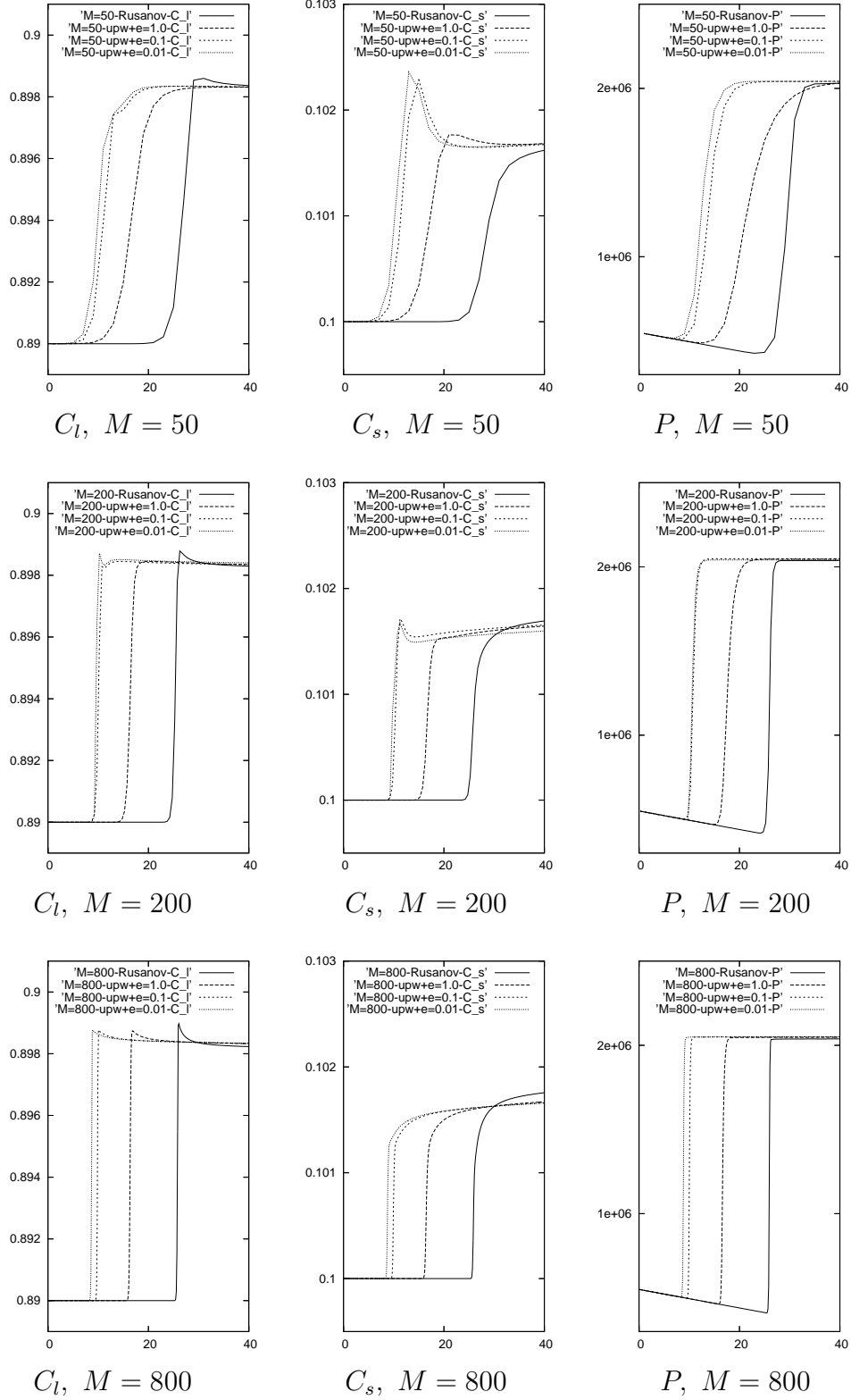
Fig. 7. Task C3, $M = 50$, $M = 200$ and $M = 800$, details of comparison of Rusanov scheme (`Rusanov`) and scheme (53) with $\epsilon = 1$ (`upw+e=1.0`), $\epsilon = 0.1$ (`upw+e=0.1`) and $\epsilon = 0.01$ (`upw+e=0.01`), distributions of C_ℓ, C_s and P at $t = 0.3$

this industrial challenging problem numerically. We tested several numerical schemes which are based on the solution of linearized Riemann problems and we observed that instabilities can cause a collapse of a calculation. These troubles may have the following reasons:

- unphysical intermediate states in the computation of the linearized Riemann problem,
- a high sensitivity of the non-conservative terms with respect to their arguments and consequently to the rounding errors namely when a non-vanishing eigenvalue of the matrix of the linearized Riemann problem has a small magnitude.

On the other hand, the Rusanov scheme and the generalized upwind scheme with an artificial dissipative term (53) solved very well the steady as well as the unsteady flow problems. These schemes do not evaluate directly the solution of the linearized Riemann problem and therefore, do not suffer from the instability mentioned above. The presented numerical examples show that it is not easy to design a reliable numerical scheme for a non-conservative system ignoring completely the non-conservative equivalent of the Rankine-Hugoniot jump conditions. Various 'upwind-like' schemes produce different results and one has no clue as to what is physically reasonable, since the numerical results all look plausible. In order to obtain a unique solution, we have to add some extra information. There should be taken into account a more physical character of the model. This is a subject for the future research.

References

[1] E. Bournaski, I. Ivanov, Unsteady slurry pipe flow with virtual mass effect, institute of Water Problems, Sofia, Bulgaria.

[2] G. Vogel, W. Bechteler, H.-B. Kleeberg, H. Teichmann, H.-J. Vollmers, Instationäre Strömung von Wasser-Feststoff-Gemischen in Druckrohrleitungen, Tech. rep., Hochschule der Bundeswehr München, Mitteilungen Institut für Wasserwesen (1983).

[3] V. V. Rusanov, Calculation of interaction of non-steady shock waves with obstacles, J. Comp. Math. Phys. USSR 1 (1961) 267–279.

[4] V. Dolejší, T. Gallouët, On a numerical simulation of three-phase flow with a virtual mass effect, Engineering Mechanics 12 (6) (2005) 1–13.

[5] V. Dolejší, T. Gallouët, On finite volume schemes for nonconservative hyperbolic problems. In F. Bankhaldoun, D. Ouzar, S. Raghay (eds): Finite volumes for complex applications IV, Problems & Perspectives, Hermes Science Publishing, London (2005) 295–304.

[6] L. Sainsaulieu, Traveling waves solution of convection-diffusion systems whose convection terms are weakly nonconservative: application to the modeling of two-phase fluid flows, SIAM J. Appl. Math. 55 (6) (1995) 1552–1576.

[7] L. Sainsaulieu, Traveling-wave solutions of convection-diffusion systems in nonconservation form, SIAM J. Math. Anal. 27 (5) (1996) 1286–1310.

[8] E. Godlewski, P. A. Raviart, Numerical Approximation of Hyperbolic Systems of Conservation Laws, Vol. 118 of Applied Mathematical Sciences, Springer, New York, 1996.

[9] R. LeVeque, Numerical methods for conservation laws. Lectures in Mathematics ETH Zürich., Birkhäuser Verlag, Basel, 1990.

[10] R. LeVeque, Finite Volume Methods for Hyperbolic Problems, Cambridge University Press, 2002.

[11] E. F. Toro, Riemann Solvers and Numerical Methods for Fluid Dynamics, Springer-Verlag, Berlin, 1997.

[12] E. F. Toro, R. C. Millington, L. A. M. Nejad, Towards very high order Godunov schemes, in: E. F. Toro (Ed.), Godunov methods. Theory and applications, Kluwer Academic/ Plenum Publishers, 2001, pp. 907–940.

[13] P. L. Roe, Approximate Riemann solvers, parameter vectors, and difference schemes, J. Comput. Phys. 43 (2) (1981) 357–372.

[14] I. Toumi, A weak formulation of Roe's approximate Riemann solver, J. Comput. Phys. 102 (1992) 360–373.

[15] I. Toumi, A. Kumbaro, An approximate linearized Riemann solver for a two-fluid model, J. Comput. Phys. 124 (2) (1996) 286–300.

[16] J. M. Ghidaglia, A. Kumbaro, G. L. Coq, On the numerical solution to two fluid models via a cell centered finite volume method, European Journal of Fluid Mechanics B/Fluids 20 (6) (2001) 841–867.

[17] J. M. Ghidaglia, G. L. Coq, I. Toumi, Two flux schemes for computing two phase flows through mutidimensional finite volume methods., in: Proceedings of the NURETH-9 conference, American Nuclear Society, San Francisco, 1999.

[18] J. M. Masella, I. Faille, T. Gallouët, On an approximate Godunov scheme, Int. J. Comput. Fluid Dyn. 12 (2) (1999) 133–149.

[19] T. Buffard, T. Gallouët, J. M. Hérard, A sequel to a rough Godunov scheme: Application to real gases, Computers and Fluids 29 (7) (2000) 813–847.

[20] T. Gallouët, J. M. Hérard, N. Seguin, Some approximate Godunov schemes to compute shallow-water equations with topography, Comput. Fluids 32 (4) (2003) 479–513.

[21] T. Gallouët, J. M. Hérard, N. Seguin, Numerical modeling of two-phase flows using the two-fluid two-pressure approach, Math. Models Methods Appl. Sci. 14 (5) (2004) 663–700.

[22] I. Faille, E. Heintze, A rough finite volume scheme for modeling two-phase flow in a pipeline, Comput. Fluids 28 (2) (1999) 213–241.

[23] G. D. Maso, P. LeFloch, F. Murat, Definition and weak stability of nonconservative products, J. Math. Pures Appl. 74 (6) (1995) 483–548.

[24] J. F. Colombeau, A. Heibig, Nonconservative products in bounded variation functions, SIAM J. Math. Anal. 23 (4) (1992) 941–949.

[25] J. M. Greenberg, A. Y. Leroux, A well-balanced scheme for the numerical processing of source terms in hyperbolic equations, SIAM J. Numer. Anal. 33 (1) (1996) 1–16.

[26] L. A. Gosse, A well-balanced flux-vector splitting scheme designed for hyperbolic systems of conservation laws with source terms, Comput. Math. Appl. 39 (9-10) (2000) 125–159.

[27] C. Parès, M. Castro, On the well-balance property of Roe's method for nonconservative hyperbolic systems. Application to shallow-water systems., M2AN 38 (5) (2004) 821–852.

[28] T. Gallouët, Hyperbolic equations and systems with discontinuous coefficients or source terms, In Proceeding of Equadiff-11 conference, (to appear).

[29] S. R. Chakravarthy, D. A. Anderson, M. D. Salas, The split coefficient matrix method for hyperblic systems of gas dynamics equations", in: AIAA 19th Aerospace meeting, 1980, pp. AIAA paper 80–0268.

[30] T. Gallouët, J. M. Hérard, N. Seguin, On the use of symmetrizing variables for vacuum, Calcolo 40 (3) (2003) 163–194.

[31] B. Einfeldt, C. D. Munz, P. L. Roe, B. Sjögreen, On Godunov-type methods near low densities, J. Comput. Phys. 92 (1991) 273–295.